EQUATORIALLY TRAPPED WAVES IN A BACKGROUND MERIDIONAL SHEAR

16B.3

Maryam Namazi *

Boualem Khouider

Department of Mathematics and Statistics, University of Victoria, Victoria, BC, Canada

Unpublished manuscript

* *Corresponding author address:* Department of mathematics and statistics, University of Victoria, PO BOX 3045 STN CSC Victoria, B.C. Canada V8W 3P4, E-mail: maryamn@uvic.ca

ABSTRACT

The equatorial atmosphere harbours a large spectrum of waves that are trapped near and travel along the equator. These equatorially trapped waves interact nonlinearly with each other and with the planetary-barotropic waves. Here, we consider advected shallow water equations that represent interactions of these equatorial waves with a prescribed meridional-barotropic shear. We show that in the presence of an easterly shear, the eigenfrequencies of westward propagating waves decrease compared to their free analogues. The effect is more significant for larger wavenumbers. However, for most eastward going waves with high wavenumbers, the eigenfrequencies increase compared to the shear-free case. We emphasize the case of Kelvin waves, which are believed to play a central role in organized tropical convective systems. We demonstrate that unlike their free analogues that have no meridional velocity, the shear-forced Kelvin waves exhibit a weak meridional velocity, which, nevertheless, induces a large contribution to the flow convergence as observed in nature. Low-level convergence of moisture is believed to play a central role in sustaining moist convection in tropical convective systems. In addition, the shear-Kelvin wave interaction excites three other equatorial waves: a Rossby wave, eastward and westward gravity waves of weaker strength but their phase speeds and wave structures despite some quantitative differences, resemble those of the dry waves. We show that the effect of the shear is more significant for larger wavenumbers and/or stronger shears. Furthermore, we look at the interactions between the meridional shear and other equatorial waves. We show that the westerly shear makes the westward Yannai wave and some Rossby waves unstable and interestingly the stable Rossby waves move eastward rather than westward. We demonstrate that in the sheared environment some waves are more/less trapped near the equator than their free

counterparts. This can significantly modify the way in which the equatorial waves interact with the extratropical waves, i.e. the tropical-extratropical interactions and teleconnection patterns of weather and climate.

1. Introduction

Most of the Earth's energy intake from the sun is absorbed within the tropical belt and then redistributed to the rest of the globe through various atmospheric and oceanic flow patterns. The organized deep convection is a major source of the energy for tropical circulations derived by latent heat associated with the phase change of water in the tropics. Therefore, the study of tropical dynamics is essential for understanding the climate system and for improving climate and weather prediction models and it is a topic of interest for the past few decades. However, the general circulation models (GCM's) represent poorly the Madden-Julian oscillation (MJO) and the convectively coupled waves which are believed to impact the mid-latitude weather and climate. These equatorial waves are trapped near the equator and travel along it and they interact nonlinearly with each other and with the extra-tropical waves. Thus, in order to understand the interaction between these equatorial waves and the extra-tropics some simplified models are developed to capture the main features of these dynamics.

In this work we are interested in the interactions of these equatorial waves with two barotorpic background shears; an equatorial easterly and an equatorial westerly wind mimicking the zonal wind in winter at 200 mb, over the western Pacific ocean and eastern Pacific ocean respectively, Zhang and Webster (1989). In section 2, we use the two mode model,

representing the interactions between the barotorpic (vertically averaged) mode and the first baroclinic mode obtained by Galerkin projection of the hydrostatic beta-plane primitive equations (Majda and Biello 2003). In section 3, we solve the forced baroclinic wave system numerically by applying a meridional Galerkin projection introduced by Khouider and Majda (2001) which gives a one dimensional advected system.

In section 4, we do linear analysis of the meridionally projected system by assuming wavelike solutions that travel zonally along the equator. We compare the frequencies and the meridional structures of the forced waves with their free analogues. We show that in the sheared environment, the frequencies of most of the eastward waves are increased while for the westward waves, they are decreased. In addition, westward mixed Rossby-gravity (MRG) waves and some Rossby waves become unstable in the presence of the westerly shear. We emphasize the case of Kelvin waves, which play an important role in organized tropical convective systems. Unlike their free analogues where there is no meridional velocity, the shear-forced Kelvin waves exhibit a weak meridional velocity. This weak meridional velocity leads to a flow convergence/divergence at the equator as observed in nature.

In chapter 5, we evolve the one dimensional advected system in time by using the second order central scheme of Nessyahu and Tadmor (1990) to capture the dynamical interaction of the equatorial waves with the imposed barotropic shear.The forced waves have the same frequencies and meridional structures as those obtained by the linear analysis in section 4. In addition, we demonstrate that each symmetric (anti-symmetric) equatorial wave excites other symmetric (anti-symmetric) equatorial waves with the same wavenumber which more or less resemble their free cases. In this section, we consider mainly the two cases of the forced Kelvin and Rossby waves. Moreover, due to nonlinear interaction between the waves

and exciting other waves, all of them become unstable in presence of westerly shear.

2. Simplified Model

a. Barotopic-first baroclinic model

We consider the primitive equations on an equatorial beta-plane (Majda 2003)

$$\begin{aligned} &\frac{D\mathbf{V}_H}{Dt} + \beta y \mathbf{V}_H^{\perp} = -\nabla_H P \\ &\frac{D\Theta}{Dt} + \frac{N^2\theta_0}{g} W = 0 \\ &\frac{\partial P}{\partial z} = g\frac{\Theta}{\theta_0} \\ &\mathrm{div}_H \mathbf{V}_H + W_z = 0 \end{aligned} \tag{1}$$

with rigid boundary conditions

$$w(x, y, z, t)|_{z=0,H} = 0, \tag{2}$$

where $z = 0$ corresponds to the surface of the Earth and $z = H \approx 16$km is the hight of troposphere. Here $\mathbf{V}_H = (U(x, y, z, t), V(x, y, z, t))$ is the horizontal velocity field with $\mathbf{V}_H^{\perp} = (-V, U)$, W is the vertical velocity and Θ is the potential temperature. $N = 0.01$ is the Brunt-Vaisala buoyancy frequency, $g = 9.8$ ms^{-2} is the gravitational acceleration, $\beta = 2.2804 \times 10^{-11}\mathrm{s}^{-1}\mathrm{m}^{-1}$ is the Coriolis parameter coefficient and $\theta_0 = 300$K is a reference potential temperature. In addition,

$$\frac{D}{Dt} \equiv \frac{\partial}{\partial t} + U\frac{\partial}{\partial x} + V\frac{\partial}{\partial y} + W\frac{\partial}{\partial}$$

is the material derivative and div_H, and ∇_H are the horizontal divergence and horizontal gradient respectively. We consider the crude vertical approximation (Biello and Majda 2003;

Khouider and Majda 2005)

$$\begin{pmatrix} \mathbf{V}_H \\ P \end{pmatrix}(x,y,z,t) \approx \begin{pmatrix} \bar{\mathbf{v}} \\ \bar{p} \end{pmatrix}(x,y,t) + \begin{pmatrix} \mathbf{v} \\ p \end{pmatrix}(x,y,t)\cos(\frac{\pi z}{H})$$
$$\begin{pmatrix} W \\ \Theta \end{pmatrix}(x,y,z,t) \approx \begin{pmatrix} w \\ \theta \end{pmatrix}(x,y,t)\sin(\frac{\pi z}{H}) \tag{3}$$

where the barotropic modes are the vertically averaged quantities over the height of the troposphere, H, obtained by

$$\bar{f} = \int_0^H f(z)dz.$$

Note that the barotropic components of the vertical velocity, W, and Θ vanish thanks to the rigid boundary conditions and the hydrostatic balance.

Next, the barotropic-first baroclinic system equations are obtained by applying the Galerkin projection of the primitive equations on the barotropic and first baroclinic mde. The projection on the first baroclinic mode is derived by

$$\langle f, g\rangle = \frac{1}{H}\int_0^H f(z)g(z)dz,$$

where $g(z) = \cos(\frac{\pi z}{H})$ for the horizontal velocity, $\mathbf{V}_H$, and the pressure, P and $g(z) = \sin(\frac{\pi z}{H})$ for the potential temperature, Θ, and the vertical velocity, W while the projection on the barotropic mode is obtained in the same way with $g(z) = 1$. Moreover, in the remaining of the paper, the equations are non-dimensionalized using $c = \frac{NH}{\pi} \approx 50\text{ms}^{-1}$ as velocity scale, $L = (c\beta^{-1})^{1/2} \approx 1500\text{km}$ as the length scale, $T = \frac{L}{c} \approx 8\text{h}$ as the time scale and $\bar{\alpha} = \frac{HN^2\theta_0}{\pi g} \approx 15\text{K}$ as the temperature scale. Therefore, the barotorpic-first baroclinic

interacting systems are obtained by, in non-dimensional units,

$$\frac{\partial \bar{\mathbf{v}}}{\partial} + \bar{\mathbf{v}}.\nabla\bar{\mathbf{v}} + y\bar{\mathbf{v}} + \nabla\bar{p} = -\frac{1}{2}(\mathbf{v}.\nabla\mathbf{v} + \mathbf{v}\mathrm{div}\mathbf{v})$$
$$\mathrm{div}\bar{\mathbf{v}} = 0 \tag{4}$$

and

$$\frac{\partial \mathbf{v}}{\partial t} + \bar{\mathbf{v}}.\nabla\mathbf{v} - \nabla\theta + y\mathbf{v}^{\perp} = -\mathbf{v}.\nabla\bar{\mathbf{v}} \tag{5}$$
$$\frac{\partial \theta}{\partial t} + \bar{\mathbf{v}}.\nabla\theta - \mathrm{div}\mathbf{v} = \mathbf{0},$$

respectively. Here, we are interested in the interaction of equatorially trapped waves (solution of (5) when $\bar{v} = 0$) with a prescribed barotropic flow. Thus, we consider system (5) forced by barotropic flow by assuming that the feedback of the associated baroclinic response in (4) is negligible. This is accurate to the first order approximation if this response is smaller than the imposed barotropic flow.

b. Imposed barotropic Shear background

We prescribe two barotropic shears, $\bar{\mathbf{v}} = (\bar{u}(y), 0)$ where $\bar{u}(y)$, mimics the equatorial jet stream: an equatorial easterly shear with magnitude of -10 ms^{-1} at the equator and 40 ms^{-1} in mid-latitudes which is a typical meridional distribution of the zonal wind at 200 mb over the western Pacific ocean and an equatorial westerly shear with magnitude 10 ms^{-1} at the equator and 30 ms^{-1} in mid-latitudes which is similar to the zonal wind over eastern Pacific ocean in winter at 200 mb Zhang and Webster (1989). The two zonal winds are formulated

by

$$\bar{u}_e(y) = \bar{u}_0(\frac{3}{4}y^2 - 1)\exp(-y^2/16)$$
$$\bar{u}_w(y) = \bar{u}_0(\frac{5}{12}y^2 + 1)\exp(-y^2/16)$$

where $\bar{u}_0$ is the strength of the wind at the equator fixed to 10 ms^{-1}. The meridional distribution of these prescribed shears are shown in figure (1). By considering this barotropic shear, system (5) simplifies to

$$\begin{aligned}
&\frac{\partial u}{\partial t} + \bar{u}(y)\frac{\partial u}{\partial x} - yv - \frac{\partial \theta}{\partial x} = -v\frac{\partial \bar{u}}{\partial y}(y)\\
&\frac{\partial v}{\partial t} + \bar{u}(y)\frac{\partial v}{\partial x} + yu - \frac{\partial \theta}{\partial y} = 0\\
&\frac{\partial \theta}{\partial t} + \bar{u}(y)\frac{\partial \theta}{\partial x} - (\frac{\partial u}{\partial x} + \frac{\partial v}{\partial y}) = 0.
\end{aligned} \tag{6}$$

In previous work (Ferguson et al., 2009), we have shown that the effect of the wind on equatorially trapped waves, is mainly due to gradient of the wind. A constant zonal wind has no other effect than just the obvious Doppler shift.

Note that Zhang-Webster studied the effect of these two shears, a westerly and an easterly wind, using the shallow water equations introduced by Matsuno (1966) on an equatorial beta-plane

$$\begin{aligned}
&\frac{\partial u}{\partial t} + \bar{u}(y)\frac{\partial u}{\partial x} - yv - \frac{\partial \theta}{\partial x} + v\frac{\partial \bar{u}}{\partial y} = 0,\\
&\frac{\partial v}{\partial t} + \bar{u}(y)\frac{\partial v}{\partial x} + yu - \frac{\partial \theta}{\partial y} = 0,\\
&\frac{\partial \theta}{\partial t} + \bar{u}(y)\frac{\partial \theta}{\partial x} + y\bar{u}(y)v - (\frac{\partial u}{\partial x} + \frac{\partial v}{\partial y}) = 0.
\end{aligned} \tag{7}$$

which is similar to the shallow water equation derived by projecting primitive equations into the barotropic-first baroclinic mode except for the extra term $y\bar{u}(y)v$ in the potential

temperature equation, θ. To seek for wave-like solutions that move along the equator, Zhang and Webster (1989) expanded the governing equations (7) in terms of the first few equatorially trapped waves of Matsuno (1966), that are solutions to linear-enforced equations when $\bar{u}(y) = 0$.

Here, we extend this methodology by using a more general and simpler treatment where the the solutions are Galerkin projected in the meridional direction onto the parabolic cylinder functions. In addition to the more standard linear theory, in order to capture the dynamical interactions between the barotropic mode and these equatorial waves, we evolve the meridionally projected system, from an initial state consistent of a given wave-mode solution by a direct integration using the high-order numerical scheme, the central scheme of Nessyahu and Tadmor (1989). Interestingly, these interactions excite other equatorial waves as we will discuss in section 5.

c. Energy source and energy sink

Here, we consider a channel along the equator with periodic boundary condition in zonal direction and the walls located at $Y_0 = 5000$km north and south of the equator. The kinetic energy associated with the first baroclinic mode is

$$E_c(t) = \frac{1}{2}\int_{-Y_0}^{Y_0}\int_0^X u^2 + v^2 + \theta^2 dxdy \tag{8}$$

therefore, the energy tendency is given by

$$\frac{d}{dt}E_c(t) = -2(\int_0^X v\theta\Big|_{Y_0} dx + \int_0^{Y_0}\int_0^X uv\frac{\partial\bar{u}}{\partial y}dxdy) \tag{9}$$

using the fact that the barotropic flow is non-divergent and periodic boundary conditions

in the zonal direction. This shows that the energy tendency depends on the interaction between u, v and the gradient of the barotropic wind (interaction energy tendency) and also depends on the structure of the wave at the channel walls (boundary energy tendency). This kinetic energy is conserved if the barotropic wind is constant and if the waves are sufficiently trapped around the equator. Therefore, for a forced wave which is not sufficiently trapped, the Dirichlet boundary condition is not a reasonable assumption.

3. Numerical methodology

In this section, we present an efficient numerical strategy for equatorial waves; introduced by Khouider and Majda (2001), to approximate system (6) numerically based on the Galerkin projection in the meridional direction onto the parabolic cylinder functions. First, we review parabolic cylinder functions and their properties, Hermite polynomials and Gauss-Hermite quadrature. Then, we apply the meridional truncation strategy to simplify the two dimensional advected shallow water equations (6) to a one dimensional non-homogeneous advection system. Then, we solve the obtained system by the 2nd order non-staggered central scheme introduced by Nessyahu and Tadmor (1989). Finally, we present the properties of the equatorial waves, like their trapping and phase speed, in a sheared environment.

a. Parabolic cylinder functions and Gauss-Hermite quadrature

Parabolic cylinder functions are the well-known solutions of the harmonic oscillator

$$\frac{\partial^2}{\partial \eta^2} f(\eta) + \frac{1}{2}(2m + 1 - \frac{\eta^2}{2}) f(\eta) = 0 \tag{10}$$

which are given by

$$D_m(\eta) = 2^{-m/2} H_m(\frac{\eta}{\sqrt{2}}) e^{-\eta^2/4} \tag{11}$$

where Hermite polynomials, $H_m(\xi)$, are defined by

$$H_m(\xi) = (-1)^m e^{\xi^2} \frac{d^m e^{-\xi^2}}{d\xi^m} \quad \text{for} \;\; m = 0, 1, \cdots .$$

They are obtained by the following recursive formula

$$H_{j+1}(\xi) - 2\xi H_j(\xi) + 2j H_{j-1}(\xi) = 0, \quad H_0(\xi) = 1, \;\; H_1(\xi) = 2\xi.$$

In addition, they form an orthonormal basis for square integrable functions. If $\phi_N(y) = (N!\sqrt{\pi})^{-\frac{1}{2}} D_N(\sqrt{2}y)$, then

$$(\phi_N, \phi_M) = \int_{-\infty}^{\infty} \phi_N(y)\phi_M(y) d(y) = \delta_{N,M}. \tag{12}$$

We introduce the lowering and raising operators of quantum mechanics. Then,

$$\begin{aligned} L_-\phi_N(y) &= -(2(N+1))^{1/2}\phi_{N+1}(y), \\ L_+\phi_N(y) &= (2N)^{1/2}\phi_{N-1}(y). \end{aligned}$$

The Gauss-Hermite quadrature is formulated by

$$\int_{-\infty}^{\infty} F(y)dy = \sum_{j=1}^{N} F(y_j)\bar{H}_j, \quad \bar{H}_j = H_j e^{y_j^2}, \quad j = 1, \cdots, N \tag{13}$$

where $y_j, j = 1, 2, \cdots, N$ are the N zeros of the Hermite polynomial H_N for a given N and H_j's are the standard Hermite-Gauss quadrature coefficient given by

$$H_j = \frac{2^{N-1} N! \sqrt{\pi}}{N^2 (H_{N-1}(y_j))^2}.$$

See Ralston (1987) for more details. This approximation is exact if $F(y) = p_{2N-1}(y)e^{-y^2}$ where p_{2N-1} is a polynomial of degree $2N-1$. Therefore, the parabolic cylinder functions form an orthonormal basis for $L^2(\mathbb{R}^2)$ with the discrete inner product,

$$\langle f, g\rangle_N = \sum_{j=1}^{N} f(y_j)g(y_j)\bar{H}_j,$$

which means

$$\langle \phi_m, \phi_l\rangle_N = \delta_{ml}, \quad 0 \le m, l \le N-1. \tag{14}$$

Therefore, for any given function $f \in L^2(\mathbb{R}^2)$, the Hermite interpolation is defined as the projection onto the discrete space spanned by the orthonormal basis $\phi_l, l = 0, \ldots, N-1$. We set,

$$P_N f(y) = \sum_{l=0}^{N-1} \tilde{f}_l \phi_l(y), \tag{15}$$

where $\tilde{f}_l = \langle f, \phi_l\rangle_N, \quad l = 0, \ldots, N-1$. Thus, this approximation is exact, $P_N f = f$, if f is in the form $p_{N-1}e^{-y^2/2}$.

b. Galerkin Projection and its application to shallow water equations

For any given square integrable function $u(y)$, we use the low order meridional projection described above to write u in terms of the discrete orthonormal basis function ϕ_l, i.e.,

$$u(y) \approx P_N u(y) = \sum_{l=0}^{N-1} \tilde{u}_l \phi_l(y), \quad \text{for } \tilde{u}_l = \langle u, \phi_l\rangle_N, \quad l = 0, \ldots, N-1. \tag{16}$$

By using the lowering and rising operators and their identities, we write an explicit

formula for $P_N\frac{\partial}{\partial y}P_N u$,

$$\begin{aligned} P_N\frac{\partial}{\partial y}P_N u &= P_N\sum_{l=0}^{N-1}\frac{1}{2}\tilde{u}_l(L_+ + L_-)\phi_l(y) \\ &= P_N\sum_{l=0}^{N-1}\frac{1}{\sqrt{2}}\tilde{u}_l(l^{1/2}\phi_{l-1}(y) - (l+1)^{1/2}\phi_{l+1}(y)) \\ &= \sum_{l=0}^{N-1}\frac{1}{\sqrt{2}}(\tilde{u}_{l+1}(l+1)^{1/2} - \tilde{u}_{l-1}l^{1/2})\phi_l(y) \end{aligned} \tag{17}$$

and similarly,

$$P_N y P_N u(y) = \sum_{l=0}^{N-1}\frac{1}{\sqrt{2}}(\tilde{u}_{l+1}(l+1)^{\frac{1}{2}} + \tilde{u}_{l-1}l^{\frac{1}{2}})\phi_l(y) \tag{18}$$

where we use $P_N\phi_l = \phi_l$ for $l = 0, \cdots, N-1$, $P_N\phi_N \equiv 0$ and also the convention $\tilde{u}_{-1} = \tilde{u}_N \equiv 0$.

For the first equation of system (6),

$$\frac{\partial u}{\partial t} + \bar{u}(y)\frac{\partial u}{\partial x} - yv - \frac{\partial \theta}{\partial x} = -v\frac{\partial \bar{u}}{\partial y} \tag{19}$$

we project u, v and θ onto the first N meridional modes, i.e,

$$\begin{pmatrix} u \\ v \\ \theta \end{pmatrix}(x,y,t) = \sum_{l=0}^{N-1}\begin{pmatrix} \tilde{u}_l \\ \tilde{v}_l \\ \tilde{\theta}_l \end{pmatrix}(x,t)\phi_l(y)$$

where

$$\tilde{f}_l(x,t) = \sum_{j=1}^{N} f(x,y_j,t)\phi_l(y_j)\bar{H}_j.$$

So, we rewrite equation (19) in discrete form

$$\sum_{l=0}^{N-1}\left[\frac{\partial \tilde{u}_l}{\partial t} + \bar{u}(y)\frac{\partial \tilde{u}_l}{\partial x} - \frac{\partial \tilde{\theta}_l}{\partial x} - [y - \bar{u}_y]\tilde{v}_l\right]\phi_l(y) = 0 \tag{20}$$

and we take the following integral on y-direction,

$$\int_{-\infty}^{\infty}\phi_m(y)\left(\sum_{l=0}^{N-1}\left[\frac{\partial\tilde{u}_l}{\partial t}+\bar{u}(y)\frac{\partial\tilde{u}_l}{\partial x}-\frac{\partial\tilde{\theta}_l}{\partial x}-[y-\bar{u}_y]\tilde{v}_l\right]\phi_l(y)\right)dy=0 \tag{21}$$

for $m\in\{0,\cdots,N-1\}$. By using the orthonormality (14) and identity (18), we get

$$\frac{\partial\tilde{u}_m}{\partial t}+\sum_{l=0}^{N-1}\frac{\partial\tilde{u}_l}{\partial x}\int_{-\infty}^{\infty}\bar{u}(y)\phi_m(y)\phi_l(y)dy-\frac{\partial\tilde{\theta}_m}{\partial x}-\frac{1}{\sqrt{2}}(\tilde{v}_{m+1}(m+1)^{1/2}+\tilde{v}_{m-1}(m)^{1/2})$$
$$+\sum_{l=0}^{N-1}\tilde{v}_l\int_{-\infty}^{\infty}\bar{u}_y\phi_m(y)\phi_l(y)dy=0. \tag{22}$$

If we set

$$\bar{u}_{m,l}=\int_{-\infty}^{\infty}\bar{u}(y)\phi_m(y)\phi_l(y)dy=\sum_{j=1}^{N}\bar{u}(y_j)\phi_m(y_j)\phi_l(y_j)H_je^{y_j^2},$$

and

$$\hat{u}_{m,l}=\int_{-\infty}^{\infty}\bar{u}_y(y)\phi_m(y)\phi_l(y)dy=\sum_{j=1}^{N}\bar{u}_y(y_j)\phi_m(y_j)\phi_l(y_j)H_je^{y_j^2},$$

then equation (22) can be formulated as

$$\frac{\partial\tilde{u}_m}{\partial t}+\sum_{l=0}^{N-1}\frac{\partial\tilde{u}_l}{\partial x}\bar{u}_{m,l}-\frac{\partial\tilde{\theta}_m}{\partial x}-\frac{1}{\sqrt{2}}(\tilde{v}_{m+1}(m+1)^{1/2}+\tilde{v}_{m-1}(m)^{1/2})+\sum_{l=0}^{N-1}\tilde{v}_l\hat{u}_{m,l}=0. \tag{23}$$

Similarly, we write the second and third equations in (6) in discrete form

$$\frac{\partial\tilde{v}_m}{\partial t}+\sum_{l=0}^{N-1}\frac{\partial\tilde{v}_l}{\partial x}\bar{u}_{m,l}-\frac{1}{\sqrt{2}}(\tilde{\theta}_{m+1}(m+1)^{1/2}-\tilde{\theta}_{m-1}(m)^{1/2})$$
$$+\frac{1}{\sqrt{2}}(\tilde{u}_{m+1}(m+1)^{1/2}+\tilde{u}_{m-1}(m)^{1/2})=0, \tag{24}$$
$$\frac{\partial\tilde{\theta}_m}{\partial t}+\sum_{l=0}^{N-1}\frac{\partial\tilde{\theta}_l}{\partial x}\bar{u}_{m,l}-\frac{\partial\tilde{u}_m}{\partial x}-\frac{1}{\sqrt{2}}(\tilde{v}_{m+1}(m+1)^{1/2}-\tilde{v}_{m-1}(m)^{1/2})=0. \tag{25}$$

Therefore, primitive equations on the beta-plane (6) can be written as a one-dimensional advection system,

$$\frac{\partial\tilde{W}}{\partial t}+A\frac{\partial\tilde{W}}{\partial x}+(B+C)\tilde{W}=0 \tag{26}$$

where $\tilde{W} = (\tilde{u}_0, \cdots, \tilde{u}_{N-1}, \tilde{v}_0, \cdots, \tilde{v}_{N-1}, \tilde{\theta}_0, \cdots, \tilde{\theta}_{N-1})'$ and the constant coefficient matrices $A, B, C \in M_{3N\times 3N}$ are given by

$$A = \begin{pmatrix} A_1 & 0 & -I_N \\ 0 & A_1 & 0 \\ -I_N & 0 & A_1 \end{pmatrix}, \; B = -\frac{1}{\sqrt{2}} \begin{pmatrix} 0 & B_1 & 0 \\ -B_1 & 0 & B_2 \\ 0 & B_2 & 0 \end{pmatrix}, \; C = \begin{pmatrix} 0 & C_1 & 0 \\ 0 & 0 & 0 \\ 0 & 0 & 0 \end{pmatrix}$$

where

$$A_1 = \begin{pmatrix} \bar{u}_{0,0} & \bar{u}_{0,1} & \cdots & \bar{u}_{0,N-1} \\ \bar{u}_{1,0} & \bar{u}_{1,1} & \cdots & \bar{u}_{1,N-1} \\ \vdots & & & \\ \bar{u}_{N-1,0} & \bar{u}_{N-1,1} & \cdots & \bar{u}_{N-1,N-1} \end{pmatrix}, \; I_N = \begin{pmatrix} 1 & 0 & \cdots & 0 \\ 0 & 1 & \cdots & 0 \\ \vdots & & \ddots & \\ 0 & 0 & \cdots & 1 \end{pmatrix},$$

$$B_1 = \begin{pmatrix} 0 & 1 & 0 & & 0 \\ 1 & 0 & \sqrt{2} & & \\ & \sqrt{2} & \ddots & \ddots & \\ & & \ddots & 0 & \sqrt{N-1} \\ 0 & & \sqrt{N-1} & & 0 \end{pmatrix}, \; B_2 = \begin{pmatrix} 0 & 1 & 0 & & 0 \\ -1 & 0 & \sqrt{2} & & \\ & -\sqrt{2} & \ddots & \ddots & \\ & & \ddots & 0 & \sqrt{N-1} \\ 0 & & -\sqrt{N-1} & & 0 \end{pmatrix},$$

$$C_1 = \begin{pmatrix} \hat{u}_{0,0} & \hat{u}_{0,1} & \cdots & \hat{u}_{0,N-1} \\ \hat{u}_{1,0} & \hat{u}_{1,1} & \cdots & \hat{u}_{1,N-1} \\ \vdots & & & \\ \hat{u}_{N-1,0} & \hat{u}_{N-1,1} & \cdots & \hat{u}_{N-1,N-1} \end{pmatrix}.$$

c. Radiation condition

In order to avoid spurious waves introduced by numerical approximation, we need to impose the following radiation conditions proposed by Majda-Khouider (2001), i,e.

$$\tilde{v}_{N-1} = 0, \tilde{\theta}_{N-1} = -\tilde{u}_{N-1}, \tilde{\theta}_{N-2} = -\tilde{u}_{N-2}. \tag{27}$$

If we neglect the forcing terms in equations (23)-(25), we get

$$\frac{\partial \tilde{u}_k}{\partial t} - \frac{\partial \tilde{\theta}_k}{\partial x} - \frac{1}{\sqrt{2}}(\tilde{v}_{k+1}(k+1)^{1/2} + \tilde{v}_{k-1}(k)^{1/2}) = 0, \tag{28}$$

$$\frac{\partial \tilde{v}_k}{\partial t} - \frac{1}{\sqrt{2}}(\tilde{\theta}_{k+1}(k+1)^{1/2} - \tilde{\theta}_{k-1}(k)^{1/2}) + \frac{1}{\sqrt{2}}(\tilde{u}_{k+1}(k+1)^{1/2} + \tilde{u}_{k-1}(k)^{1/2}) = 0, \tag{29}$$

$$\frac{\partial \tilde{\theta}_k}{\partial t} - \frac{\partial \tilde{u}_k}{\partial x} - \frac{1}{\sqrt{2}}(\tilde{v}_{k+1}(k+1)^{1/2} - \tilde{v}_{k-1}(k)^{1/2}) = 0. \tag{30}$$

By using the radiation condition $\tilde{v}_{N-1} = 0$ for $k = N-1$ in equation (29), we get the radiation condition $\tilde{\theta}_{N-2} = -\tilde{u}_{N-2}$. Therefore, we omit this equation for $N-1$ in system (26) and also this equation for $k = N-2, N-3$ becomes

$$\frac{\partial \tilde{v}_k}{\partial t} + \frac{2}{\sqrt{2}}\tilde{u}_{k+1}(k+1)^{1/2} + \frac{k^{1/2}}{\sqrt{2}}(\tilde{u}_{k-1} + \tilde{\theta}_{k-1}) = 0. \tag{31}$$

However, equations (28) and (30) lead to the two conflicting equations

$$\frac{\partial \tilde{u}_k}{\partial t} + \frac{\partial \tilde{u}_k}{\partial x} - \frac{1}{\sqrt{2}}(\tilde{v}_{k+1}(k+1)^{1/2} + \tilde{v}_{k-1}(k)^{1/2}) = 0,$$

$$\frac{\partial \tilde{u}_k}{\partial t} + \frac{\partial \tilde{u}_k}{\partial x} + \frac{1}{\sqrt{2}}(\tilde{v}_{k+1}(k+1)^{1/2} - \tilde{v}_{k-1}(k)^{1/2}) = 0$$

for $k = N-2, N-1$ after using radiation condition $\tilde{\theta}_k = -\tilde{u}_k$. We handle this problem by averaging these equations to arrive at (Khouider and Majda 2008)

$$\frac{\partial \tilde{u}_k}{\partial t} + \frac{\partial \tilde{u}_k}{\partial x} - \frac{1}{\sqrt{2}}\tilde{v}_{k-1}(k)^{1/2} = 0. \tag{32}$$

The same holds for the forced cases with $k = N-2, N-1$ and implementing these radiation conditions to equations (23) and (25) gives

$$\frac{\partial \tilde{u}_k}{\partial t} + \sum_{l=0}^{N-1} \frac{\partial \tilde{u}_l}{\partial x} \bar{u}_{k,l} + \frac{\partial \tilde{u}_k}{\partial x} - \frac{1}{\sqrt{2}}(\tilde{v}_{k+1}(k+1)^{1/2} + \tilde{v}_{k-1}(k)^{1/2}) + \sum_{l=0}^{N-1} \tilde{v}_l \hat{u}_{k,l} = 0,$$

$$\frac{\partial \tilde{u}_k}{\partial t} - \sum_{l=0}^{N-3} \frac{\partial \tilde{\theta}_l}{\partial x} \bar{u}_{k,l} + \frac{\partial \tilde{u}_{M-2}}{\partial x} \bar{u}_{k,M-2} + \frac{\partial \tilde{u}_{M-1}}{\partial x} \bar{u}_{k,M-1} + \frac{\partial \tilde{u}_k}{\partial x} +$$

$$\frac{1}{\sqrt{2}}(\tilde{v}_{k+1}(k+1)^{1/2} - \tilde{v}_{k-1}(k)^{1/2}) - \sum_{l=0}^{N-1} \tilde{v}_l u^*_{k,l} = 0.$$

Therefore, we average these equations to get

$$\frac{\partial \tilde{u}_k}{\partial t} + \frac{1}{2} \sum_{l=0}^{N-3} (\frac{\partial \tilde{u}_l}{\partial x} - \frac{\partial \tilde{\theta}_l}{\partial x}) \bar{u}_{k,l} + \frac{\partial \tilde{u}_{M-2}}{\partial x} \bar{u}_{k,M-2} + \frac{\partial \tilde{u}_{M-1}}{\partial x} \bar{u}_{k,M-1} + \frac{\partial \tilde{u}_k}{\partial x} -$$

$$\frac{1}{\sqrt{2}} \tilde{v}_{k-1}(k)^{1/2} + \frac{1}{2} \sum_{l=0}^{N-1} \tilde{v}_l (\hat{u}_{k,l} - u^*_{k,l}) = 0. \tag{33}$$

d. Free waves

For the free case, with no barotropic shear, we analytically derive the equatorially trapped waves, Majda (7), from the system (26) obtained by meridional projection. First, we introduce the known Riemann invariant variables, q and r as

$$q = \frac{1}{\sqrt{2}}(u - \theta) \quad \text{and} \quad r = -\frac{1}{\sqrt{2}}(u + \theta). \tag{34}$$

Therefore, we rewrite equations (23)-(25) in terms of q and r

$$\begin{aligned} &\frac{\partial \tilde{q}_k}{\partial t} + \frac{\partial \tilde{q}_k}{\partial x} - (k)^{1/2} \tilde{v}_{k-1} = 0 \\ &\frac{\partial \tilde{v}_k}{\partial t} + (k+1)^{1/2} \tilde{q}_{k+1} - k^{1/2} \tilde{r}_{k-1} = 0 \\ &\frac{\partial \tilde{r}_k}{\partial t} + \frac{\partial \tilde{r}_k}{\partial x} + (k+1)^{1/2} \tilde{v}_{k+1} = 0 \qquad \text{for } k = 1, 2, \ldots. \end{aligned} \tag{35}$$

These equations decouples into a hierachy of systems whose solutions are the equatorially trapped waves as follows. We have

a. Kelvin waves as the solutions to a single PDE when $k = 0$

$$\frac{\partial \tilde{q}_0}{\partial t} + \frac{\partial \tilde{q}_0}{\partial x} = 0 \tag{36}$$

b. mixed Rossby-gravity waves as the solutions of, when $k = 1$,

$$\begin{aligned} &\frac{\partial \tilde{q}_1}{\partial t} + \frac{\partial \tilde{q}_1}{\partial x} - \tilde{v}_0 = 0 \\ &\frac{\partial \tilde{v}_0}{\partial t} + \tilde{q}_1 = 0. \end{aligned} \tag{37}$$

which couples v_0 and q_1 and

c. Gravity waves and Rossby waves which are the solution of a complete system coupling q_k, v_{k-1} and r_{k-2}, for $k \geq 2$,

$$\begin{aligned} &\frac{\partial \tilde{q}_k}{\partial t} + \frac{\partial \tilde{q}_k}{\partial x} - k^{1/2}\tilde{v}_{k-1} = 0 \\ &\frac{\partial \tilde{v}_{k-1}}{\partial t} + k^{1/2}\tilde{q}_k - (k-1)^{1/2}\tilde{r}_{k-2} = 0 \\ &\frac{\partial \tilde{r}_{k-2}}{\partial t} - \frac{\partial \tilde{r}_{k-2}}{\partial x} - (k-1)^{1/2}\tilde{v}_{k-1} = 0 \quad \text{for } k \geq 2 \end{aligned} \tag{38}$$

This shows that for $N = 3$, we obtain six equatorial waves, one Kelvin wave, two MRGs and three Rossby and Gravity waves analytically and for any additional mode, N, we obtain three Rossby and Gravity waves of higher modes. Therefore, for any N, system (35) has $3N - 3$ solutions which defines the equatorially trapped waves. Therefore, this methodology of projecting onto the parabolic cylinder functions is equivalent to the projection onto the equatorially trapped normal modes of Matsuno (1966) used for example by Zhang and

Webster (1989), yet it is much simpler and more general in the sense that, it can be applied to an arbitary PDE system that depends on y.

4. Linear analysis of forced equatorially trapped waves

We consider a plane wavelike solution for system (26) on the form of

$$\tilde{W}(x,t) = \hat{W}\exp(i(kx - \omega t)) \tag{39}$$

where $i^2 = -1$, k is the zonal wavenumber and ω is the frequency. This leads to solving

$$\big[(kA - i(B+C)) - \omega I\big]\hat{W} = 0 \tag{40}$$

which requires to find the eigenvalues $\omega(k)$ and and eigenvectors $\hat{W}$ for the matrix $M = kA - i(B+C)$.

a. Constant wind

In the presence of constant wind, $\bar{u}(y) = \bar{u}_0$, the system (6) is a purely linear β-plane shallow water system advected by a constant wind. So, the solutions of this system are identical to their free counterparts with the Doppler-shifted frequencies $\hat{\omega} = \omega - k\bar{u}_0$. However, the equatorial waves are quite affected if the constant wind is applied to the shallow water equation (7) where the non-Doppler term, $v\bar{U}y$ is not zero. Zhang-Webster (1989) demonstrate analytically the effect of a constant wind is considerable for Rossby waves, moderate for westward Mixed Rossby-Gravity wave and negligible for other waves. In addition, they show that in westerlies (easterlies) the eigenfrequencies are larger (smaller) and the waves

are less (more) trapped around the equator.

b. Sheared environment

In this section, we consider the effect of the equatorial easterly and equatorial westerly shear on the equatorially trapped waves. Since the barotropic shear is symmetric in meridional direction, we can decouple system (40) into a symmetric sub-system and an anti-symmetric sub-system which helps to identify the forced equatorial waves more clearly.

1) Frequency

Here, we present the eigenfrequencies of the forced equatorial waves in the easterly flow (EE) and in the westerly flow in Figure 2 and 3 respectively. The eigenfrequncies shown are the relative frequencies including the Doppler effect since there is no obvious universal way to obtain the absolute frequencies explicitly.

For Kelvin waves the eigenfrequencies are larger in EW but smaller in EE than the frequencies of the free Kelvin wave. For the eastward Gravity wave the frequencies are increased compared to free waves for large wavenumbers and are decreased for small wavenumbers and lower meridional modes, N. This is more significant for EW shear. However, for westward Gravity waves the eigenfrequencies are decreased independent of the wavenumbers and meridional modes.

Also, for some parameter values of $\bar{u}_0$ or k, the matrix M may have non-real eigenvalues, resulting in unstable and/or damped waves. The westward mixed Rossby-Gravity waves (MRG) are stable in EE and for small wavenumber $k \leq 7$ the eigenfrequencies are smaller

while for larger wavenumbers the eigenfrequencies are greater than the free case. However, the westward MRG become unstable in EW. By letting $\omega = \omega_r + i\omega_i$ the wave solution of (39) becomes

$$\tilde{W}(x,t) = \hat{W}\exp(\omega_i t)\exp(i(kx - \omega_r t)) \tag{41}$$

where $\exp(\omega_i t)$ is the wave growth and ω_r is the wave phase. This will be discussed further later in this work. In the presence of EE, the Rossby waves, both symmetric and anti-symmetric, are stable and for higher modes the frequencies are positive with a positive k, i.e, the waves propagate eastward rather than westward in the shear background. In EW background, three Rossby waves become unstable two symmetric and one anti-symmetric and their eigenfrequencies are conjugates. Therefore, in each pair one wave is growing and one wave is damping.

There are three main differences between the results obtained by the vertical projection model compared to Zhang and Webster's results. The first difference is that for most of the Rossby waves in both EE and EW the relative direction of propagation changes sign, i.e, the waves move eastward. The second difference is that for EW some Rossby waves and the westward MRG waves become unstable. The third difference is that in eastward Gravity waves $N = 0$ with small wavenumber have smaller eigenfrequencies than their free counterparts while in Zhang-Webster they poses larger frequencies independent of wavenumber.

2) Physical structure of the forced waves

Here, we study the changes in physical structure and trapping factor of the sheared forced equatorial waves.

- Non-Kelvin aspect of Kelvin waves

Here, we provide an analytic proof of the generation of meridional velocity for Kelvin wave in presence of a background shear by introducing two new variables $\xi = yu - \frac{\partial \theta}{\partial y}$ and $\nu = y\theta - \frac{\partial u}{\partial y}$ as a measure of geostrophic unbalance which are zero for the free Kelvin waves. Thus, we rewrite the system (6) as a new system using the five variables (u, v, θ, ξ, ν) (Ferguson et al. 2009):

$$\begin{aligned}
&\frac{\partial u}{\partial t} + \bar{u}\frac{\partial u}{\partial x} - \frac{\partial \theta}{\partial x} - yv = -v\frac{\partial \bar{u}}{\partial y} \\
&\frac{\partial v}{\partial t} + \bar{u}\frac{\partial v}{\partial x} + \xi = 0 \\
&\frac{\partial \theta}{\partial t} + \bar{\theta}\frac{\partial}{\partial x} - (\frac{\partial u}{\partial x} + \frac{\partial v}{\partial y}) = 0 \\
&\frac{\partial \xi}{\partial t} + \bar{u}\frac{\partial \xi}{\partial x} - \bar{u}_y\frac{\partial \theta}{\partial x} - \frac{\partial \nu}{\partial x} = -\frac{\partial^2 v}{\partial y^2} + y^2 v + \bar{v}u + v\bar{u} - v\frac{\partial(\bar{u}y)}{\partial y} \\
&\frac{\partial \nu}{\partial t} + \bar{u}\frac{\partial \nu}{\partial x} - \bar{u}_y\frac{\partial u}{\partial x} - \frac{\partial \xi}{\partial x} = \bar{v}\theta - v + V_y \cdot \nabla \bar{u} + v\bar{u}_{yy}
\end{aligned} \tag{42}$$

A Kelvin wave with the known solutions $(u, v, \theta, \xi, \nu) = (u(x, y), 0, -u(x, y), 0, 0)$ in a background shear excites ξ through term $\bar{u}_y \frac{\partial \theta}{\partial x}$ in the fourth equation in (42) which shows the interaction of the shear gradient with the potential temperature. This ξ, induces a non-zero meridional velocity, in second equation of (42), consequently a non-zero ν. It's easy to see that the strength of this meridional velocity depends on the shear gradient and the wavenumber k through $\bar{u}_y \frac{\partial \theta}{\partial x}$. This wavenumber dependency is shown in Figure 4 as the relative strength of each components, u, v and θ obtained by $f_{\text{rel}} = \frac{\|f\|_2}{E_c}$ where

$$\|f\|_2 = \frac{1}{2}\int_{-\infty}^{\infty} f(x, y)^2 dy$$

and

$$E_c = \frac{1}{2}\int_{-\infty}^{\infty}(u^2 + v^2 + \theta^2)dy.$$

Note that this effect is more significant for the easterly shear where shear gradient is stronger compared to the westerly shear.

However, this weak meridional velocity induces remarkably strong convergence and/or divergence regions, shown in figure (5) with $k = 5$, which is consistent with the observation in (Roundy 2008). Furthermore, the normalized meridional structure of the forced Kelvin wave is shown in Figure 6 which shows the Kelvin wave becomes slightly more trapped off the equator which is negligible. Also the meridional velocity of the forced Kelvin wave is shown as an anti-symmetric function which is like the case for the symmetric equatorial waves.

- Gravity waves

  The westward Gravity waves are highly affected by both shears and their trapping is much weaker compare to the their free counterparts. The effect is more considerable in the easterly background, EE. Moreover, the meridional structures of u, v and θ are different compared to the results in Zhang and Webster (1989) especially for u and θ.

  However, in presence of EW and EE the eastward Gravity waves are generally more trapped except for the zonal velocity in EE which becomes less trapped and deformed compared to their free cases.

- Mixed Rossby Gravity wave

  As we discussed, the westward MRG becomes unstable in EW. However, as in Figure 8

the EE effect is negligible. In contrast, Zhang and Webster obtain stable MRG waves where the shear weaken the trapping of the waves around the equator.

Like in Zhang and Webster, the meridional structures of u and θ for the eastward gravity $N = 0$ are not affected in a shear environment but v is more trapped, Figure 8.

- Rossby waves

  Unlike the belief that Rossby waves modify the tropical-extra tropical energy transport by being less trapped, here we show that the forced Rossby waves with $N = 1$ in EE are more trapped. Note that the Rossby waves $N = 1$ become unstable in presence of EW. These results are different than the results in previous studies Zhang-Webster (1989).

3) Unstable equatorial waves

Here, we characterize the unstable forced waves obtained by the linear analysis in the background westerly shear. Since the frequencies of the unstable waves are conjugates, one wave grows and the other vanishes in time while they both propagate with a same phase speed. For the symmetric waves, the Rossby waves with $M = 1$ and 3 are unstable and for the anti-symmetric waves, the westward Yannai wave and Rossby wave $M = 2$ become unstable.

To justify this, we compare the of meridional structure of obtained stable forced waves with their free counterparts. In Figure 11, we compare the symmetric free Rossby waves with $M = 1, 3, 5$, and 7 with the stable symmetric forced waves. The structure of these

stable waves resemble with Rossby wave of $M = 5$ and 7 while they become more trapped. This implies that the unstable waves for symmetric waves are Rossby wave $M = 1$ and 3. Similarly, in Figure 12, we show the meridional structure of the free westward Yannai wave and Rossby waves $M = 2$, 4 an 6 on left panel and the two stable forced waves on right panel. This suggest that the Yannai wave and Rossby wave $M = 2$ are the unstable waves in westerly shear.

5. Evolution in time

In order to capture the nonlinear interactions between the barotropic mode and the first baroclinic mode, we evolve (26) in time by using the second order central scheme of Nessyahu and Tadmor (1990) for a non-homogeneous conservation law. Since A is a constant matrix we rewrite system (26) as a conservation law

$$\frac{\partial \tilde{W}}{\partial t} + \frac{\partial}{\partial x}(A\tilde{W}) = -(B + C)\tilde{W}. \tag{43}$$

The class of the high resolution central schemes of Nessyahu and Tadmor (1990) is an extension of Lax-Friedrichs scheme (LxF) which uses a high order polynomials rather than piecewise constant function at each time step to achieve high order convergence in smooth regions. The second order central scheme on the non-staggered grids is explained briefly below.

a. Second order central scheme

The second order central scheme on non-staggered grids for a balanced law

$$\frac{\partial u}{\partial t} + \frac{\partial f}{\partial x} = g(u) \tag{44}$$

is derived by the following steps.

- First, we construct a piecewise linear function on each grid cell $x_j \leq x \leq x_{j+2}$ by the given data at time t^n,

$$L_{j+1}(x, t^n) = u^n_{j+1} + (x - x_{j+1})\frac{1}{2\Delta x}u'_{j+1} \tag{45}$$

  where $\frac{1}{2\Delta x}u'_{j+1}$ is the slope.

- Second, we evolve the approximation in time by using finite-volume method on cell $[t^n, t^{n+1}] \times [x_{j-1}, x_{j+1}]$ to avoid solving the Riemann problem at the cell edges.

- Third, we reconstruct the piecewise linear function for time t^{n+1} and continue integrating.

Therefore, the approximation for u at time $t + \Delta t$ is formulated by

$$\begin{aligned}\bar{u}_j(t + \Delta t) = \frac{1}{2}[u_{j-1}(t) + u_{j+1}(t)] + \frac{1}{4}[u'_{j-1} - u'_{j+1}] - \\ \frac{\Delta t}{\Delta x}[f(u(x_{j+1}, t + \frac{\Delta t}{2})) - f(u(x_{j-1}, t + \frac{\Delta t}{2}))] + \frac{1}{2\Delta x}I_g\end{aligned} \tag{46}$$

where

$$I_g = \int_{x_{j-1}}^{x_{j+1}} \int_{t^n}^{t^{n+1}} g(u(x))dtdx. \tag{47}$$

I_g can be approximated using any explicit or implicit quadrature formula, for more details the reader is referred to Liotta and Romano (2000).

b. Dynamical interactions between equatorial waves and the barotropic shear

In this section, we present the interaction between the imposed barotropic shear with the equatorial Kelvin and Rossby waves in the case of equatorial easterlies.

- Kelvin waves

  We use the second order central scheme in (46)-(47) for system (26) with a $k = 4$ Kelvin wave as initial data in the EE shear background and we evolve it in time over 100 days. The interactions between the Kelvin waves and the barotorpic shear deform the Kelvin wave and also consistent with the linear analysis they induce a weak meridional velocity, Figure 13. We recall that, this meridional velocity produce strong convergence and/or divergence regions. In Figure 14, the time series of relative meridional wind (left panels) and relative meridional convergence $\max(v_y(x,y))/\max(u_x(x,y)v_y(x,y))$ (right panel) are plotted which shows the nine periods of the forced Kelvin wave over the period of 100 days.

  The time series of the total energy of the forced Kelvin wave and the relative contribution of each component u, v and θ to the total energy are respectively shown in (15) and (16). The time series of the total energy indicates that the forced Kelvin wave is dissipative and the period of the Kelvin wave increases from almost 9 days and 6 hours to 11 days and 2 hours. This means the forced Kevin wave has a smaller frequency compared to the free case which is seen in linear analysis. Moreover, the energy contribution of meridional velocity in average is 2 percent of the total energy which is weak compare to u and θ.

Interestingly, this forced Kelvin wave excite westward going waves as seen in Hovmoller diagram of the zonal velocity for [0-25] days in Figure 17. A Hovmoller diagram is a diagnostic tool to show the zonal propagation of waves by taking the meridionally averaged zonal velocity and plotting contours of its time series. To identify these waves, we apply spectral analysis in Figure 18 which shows three distinct strong peaks for forced Kelvin wave, $(k, \omega) = (4, 42), (4, 103)$ and (-4,11). The significant excited waves are a Rossby wave, eastward and westward Gravity waves of weaker strength but their phase speeds and wave structures despite some quantitative differences, resemble those of the dry waves, Figure 20. Note that the forced symmetric Kelvin wave with $k = 4$ excites two other symmetric equatorial waves with the same wavenumber. The energy contribution of each waves to the total energy is shown in Table 1 which shows most of the total energy, 97% is from the Kelvin wave.

We show snapshots of the contours of the potential temperature and the flow for filtered Kelvin wave in Figure 19, the eastward Gravity wave and the excited Rossby wave in Figure 20 at $t = 30$ days which is the local maximum of the relative velocity and the relative meridional convergence.

- Rossby wave

Rossby waves are subject of interest as they are believed to play a central role in the tropical-extratropical energy exchange. Therefore, here we do the same study as the Kelvin wave for the forced Rossby wave. First, by focusing on the Hovmoller diagram for [0-100] days of the forced Rossby wave, Figure 21, it can be seen that the Rossby wave excites at least two eastward waves, one fast and one slow wave.

The power spectrum of the forced Rossby wave, Figure 22, shows the excitement of other equatorial waves. Among those, a westward gravity wave, a kelvin wave and interestingly an MJO like wave. The structure of these waves are presented in Figure 23. The energy contribution of these waves to the total energy is shown in Table 2 which shows that unlike the forced Kelvin wave which maintains most of its total energy, the forced Rossby wave breaks down and looses its energy to the newly excited waves. Note the excited Kelvin wave, possesses the same properties such as a non-zero merdional velocity and the associated convergence/divergence regions as the forced Kelvin wave.

The meridional structure of components of filtered Rossby wave are shown in Figure 24 which clearly shows that shear-Rossby wave interaction makes the Rossby wave more trapped around the equator.

6. Conclusion

Here we study the interactions between equatorially trapped waves and two imposed barotropic shears in the context of simplified model. The model consists of the linear equatorial shallow water equations forced by an imposed barotropic background shear, representing the interactions between the barotropic mode and the first baroclinic mode. This barotropic-baroclinic model is derived by applying Galerkin projection on the non-hydrostatic primitive equations on the beta-plane in the vertical direction (Majda and Biello 2003). We apply a meridional projection introduced by Khouider and Majda (2001) to approximate

the obtained system numerically. We consider two background shears. One characterized by equatorial easterlies and one by equatorial westerlies, mimicking the mean zonal wind at 200 mb over the western an eastern Pacific ocean, respectively (Zhang and Webster (1989)).

We look at properties of the forced equatorial waves such as their frequencies and their trapping. We have performed a linear analysis for wave-like solutions that move along the equator as well as direct numerical integrations to capture the dynamical evolution of the waves in the presence of the background barotropic shear. In the sheared environment, the frequencies of most of the eastward waves are increased while for the westward waves, they are decreased. In addition, westward mixed Rossby-gravity (MRG) waves and some Rossby waves become unstable in the presence of the westerly shear.

For the direct integrations, we focus on Kelvin waves and equatorial Rossby waves. We demonstrate that the interaction of a Kelvin wave with a meridional-barotropic shear induce a non-zero meridional wind that forms and oscillates together with the whole flow structure. Although weak, this meridional velocity carries a significant equator-ward mass convergence which could intensify moist convection. The strength of the meridional wind depends on the zonal wavenumber and the strength of the shear gradient. Moreover, this shear-Kelvin interaction weakly excites other symmetric equatorial waves such as a Rossy wave (M=1) and an eastward gravity wave which more or less have the same properties as their free counterparts.

The equatorial Rossby waves are believed to have important role in tropical-extra tropical energy exchange by extending poleward. However, we show that their responses are different and they become equatorially less trapped in the case of the easterly background shear. Moreover, like the Kelvin waves, the shear-Rossby wave interaction excites other

symmetric equatorial waves. Among which we have a westward gravity wave, a kelvin wave and interestingly an MJO like wave with significant energy contribution.

In westerly shear case, the solution becomes unstable due to the excitation of unstable waves that eventually grow.

Acknowledgments.

This work is part of M.N's PhD thesis. The research of B.K. is supported by Natural Sciences and Engineering Research Council of Canada and Canadian Foundation for Climate and Atmospheric Science. M.N. is partly funded through these grants.

REFERENCES

[1] Ferguson, J., B. Khouider and M. Namazi, 2009: *Simple numerical models for the tropical-extra tropical interactions*, Chinese Annals of Mathematics, Series B, 30. Special Issue on the Occasion of Andrew Majda's 60th Birthday, 539–568.

[2] Khouider, B. and A. Majda, 2005: *A non-oscillatory balanced scheme for an idealized tropical climate model*, Theoretical and Computational Fluid dynamics. Part I: Algorithm and validation, 19, 331–354.

[3] Khouider, B. and A. Majda, 2008: *Equatorial convectively coupled waves in a simple multicloud model*, J. Atmos. Sci., 65, 3376-3397.

[4] Liotta, S. F., V. Romano and G. Russo, 2000: *Central scheme for balance laws of relaxation*, SIAM J. Numer. Anal., 38, No. 4, 1337–1356.

[5] Majda, A. and J. Biello, 2003: *The nonlinear interaction of barotropic and equatorial baroclinic Rossby waves*, J. Atmos. Sci., 60, 1809–1821.

[6] Majda, A. and B. Khouider, 2001: *A Numerical strategy for efficient modeling of equatorial waves*, Proc. Nat. Acad. Sci. 98, No 4, 1341–1346.

[7] Majda, A., 2003: *Introduction to PDEs and Waves for the Atmosphere and Ocean*, American Math Society.

[8] Matsuno, T., 1966: *Quasi-geostrophic motions in the equatorial area*, J. Met. Jap., 44, 25–41.

[9] Nessyahu, H. and E. Tadmor, 1990: *Non-oscillatory central differencing for hyperbolic conservation laws*, J. Comput. Phys., 87, 408–463.

[10] Ralston, A. and P. Rabinowitz, 1978: *A First course in numerical analysis*, McGraw Hill, New York.

[11] Roundy, P. E., 2008: *Analysis of convectively coupled Kelvin waves in the Indian Ocean MJO*, J. Atmos. Sci., 65, 1342-1359.

[12] Wheeler, M. and G. Kiladis 1999: *Convectively coupled equatorial waves: analysis of clouds and temperature in the wavenumber-frequency domain*, J. Atmos. Sci., 56, 374–399.

[13] Zhang, C. and P. Webster, 1989: *Effect of zonal flow on equatorially trapped waves*, J. Atmos. Sci. Vol. 46, No. 24, 3632–3652.

List of Tables

Wave	Kelvin	eastward Gravity	Rossby
Relative energy	97.92	0.97	0.62

TABLE 1. Contribution of the Kelvin wave, the eastward gravity wave and the Rossby wave excited by the forced Kelvin wave to the total energy at time $t = 30$ days.

Wave	Rossby wave $M = 1$	Rossby $M = 3$	Kelvin	westward Gravity
Relative energy	56.35	12.35	2.87	2.38

TABLE 2. Contribution of the Rossby wave (M=1), and excited westward gravity wave, Kelvin wave and the Rossby wave $M = 3$ excited by the forced Rossby wave $M = 1$ to the total energy at time $t = 30$ days.

List of Figures

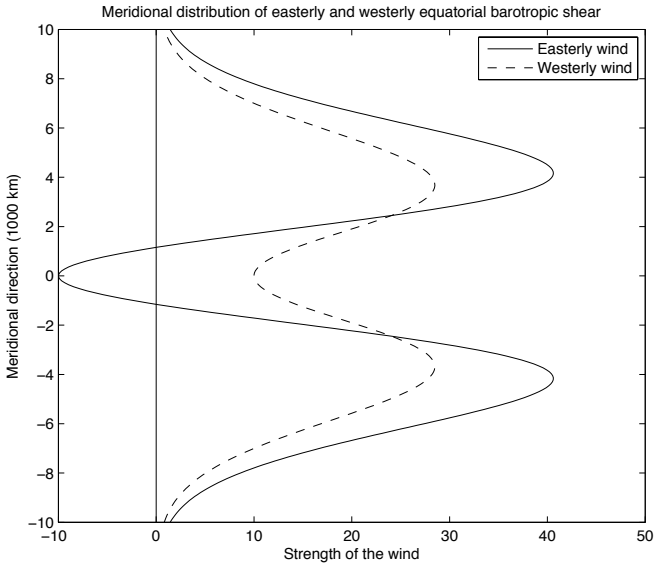

FIG. 1. Structure of equatorially easterly barotropic shear $\bar{u}_e(y)$ and equatorially westerly barotropic shear $\bar{u}_w(y)$.

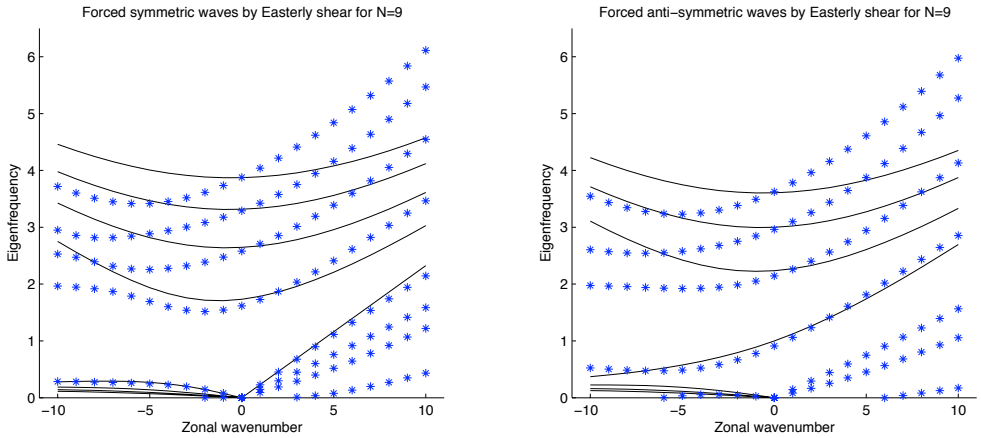

FIG. 2. Eigenfrequencies of symmetric (left panel) and anti-symmetric (right panel) equatorial waves; in no flow (solid lines) and EE (stars) background.

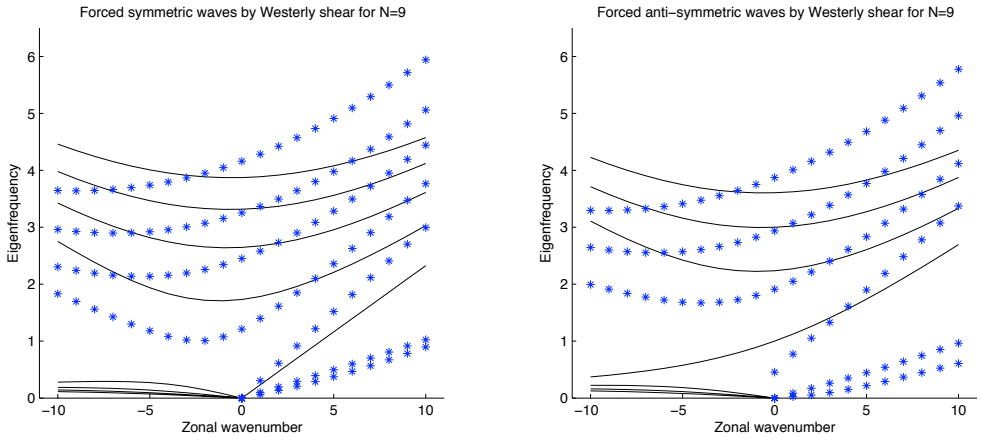

FIG. 3. Eigenfrequencies of symmetric (left panel) and anti-symmetric (right panel) equatorial waves; in no flow (solid lines) and EW (stars) background.

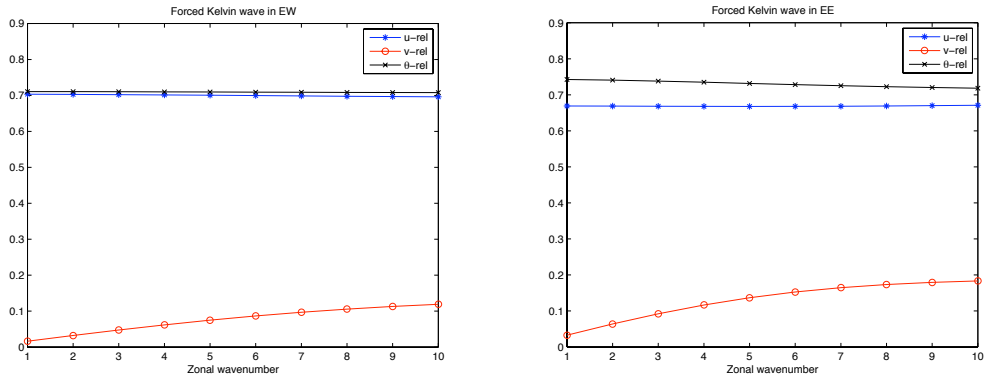

FIG. 4. Relative zonal velocity, u, relative meridional velocity, v, and relative potential temperature, θ for different wavenumbers; in equatorial westerly (EW) and in easterly (EE).

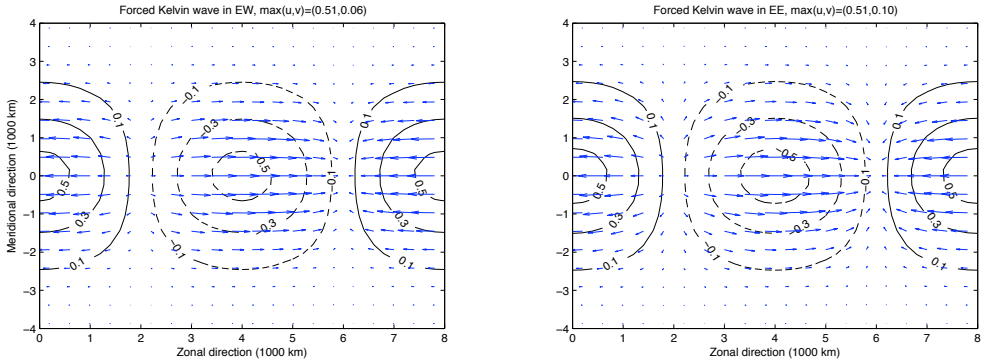

FIG. 5. Contours of potential temperature and horizontal flow for forced Kelvin wave with $k = 5$ in EW on the left panel and in EE on the right panel.

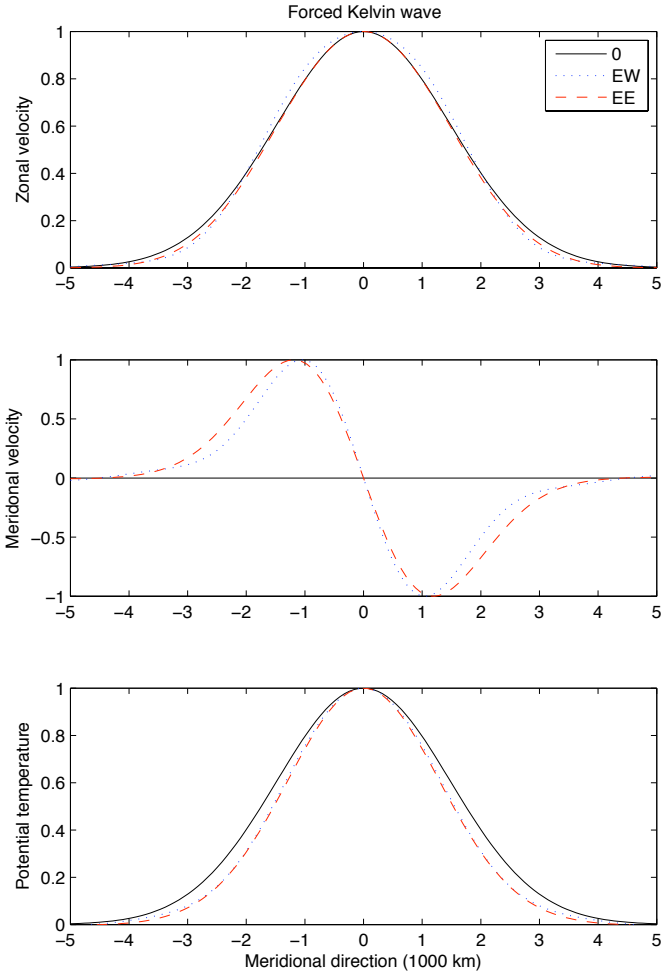

FIG. 6. Meridional structure of Kelvin wave with $k = 5$ in sheared zonal flow obtained by projected primitive equations; no wind (solid lines), westerly shear (dotted lines) and easterly shear (dashed lines).

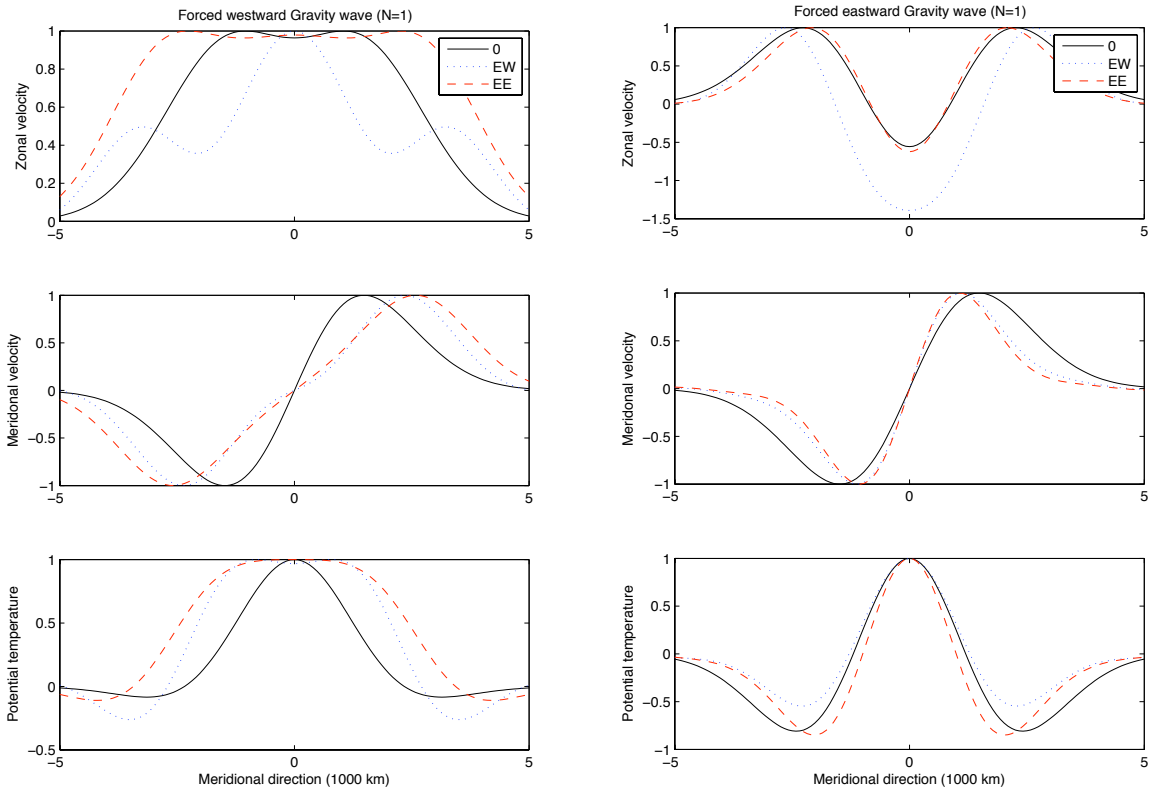

FIG. 7. Meridional structure of westward Gravity wave (left panel) and eastward Gravity wave (right panel) for $k = 5$ and $N = 1$ in sheared zonal flow obtained by projected primitive equations; no wind (solid lines), westerly shear (dotted lines) and easterly shear (dashed lines).

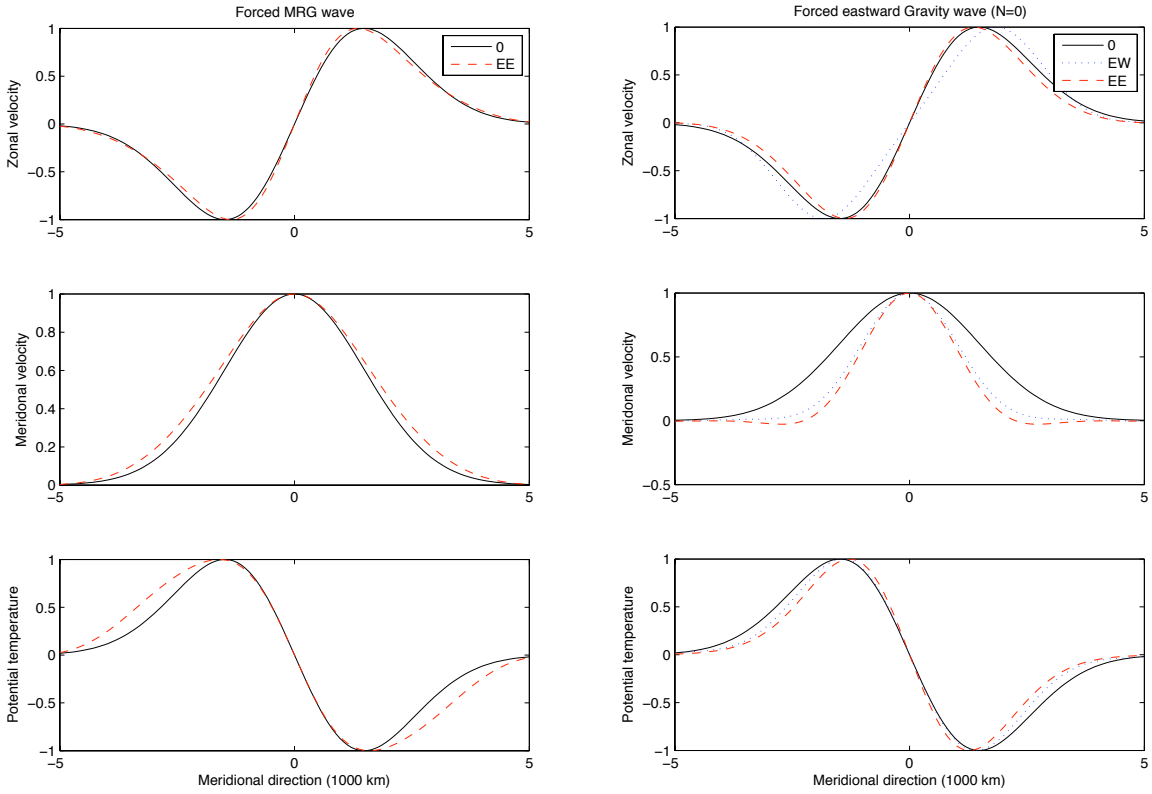

FIG. 8. Meridional structure of westward MRG wave (left panel) and eastward Gravity wave $N = 0$ (right panel) for $k = 5$ in sheared zonal flow obtained by projected primitive equations; no wind (solid lines), westerly shear (dotted lines) and easterly shear (dashed lines).

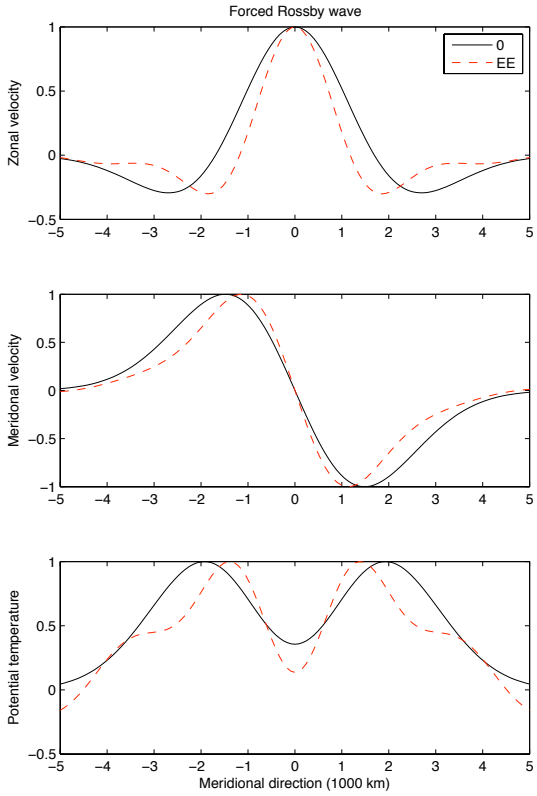

FIG. 9. Meridional structure of Rossby wave for $k = 5$ in sheared zonal flow obtained by projected primitive equations; no wind (solid lines), westerly shear (dotted lines) and easterly shear (dashed lines).

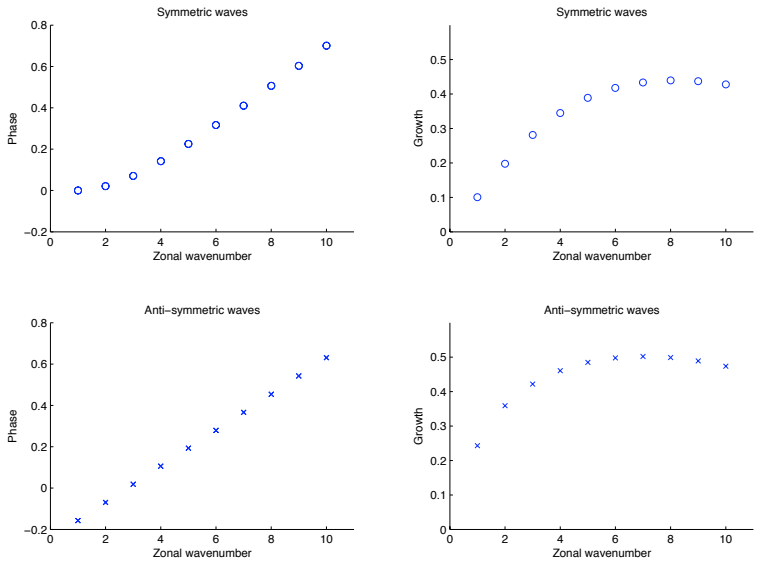

FIG. 10. phase and growth factor for symmetric unstable waves, top panels, and for anti-symmetric waves, bottom panels, for different wavenumbers.

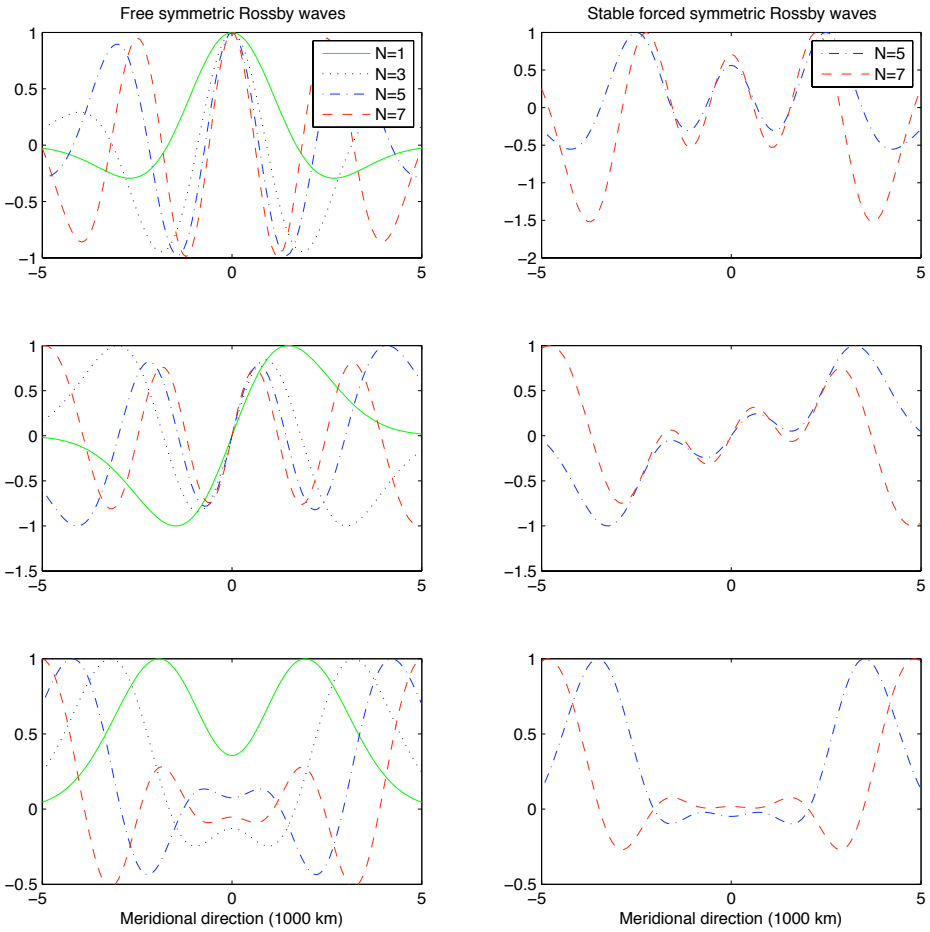

FIG. 11. Meridional structures of free symmetric Rossby waves with $M = 1, 3, 5$ and 7 on the left side and the stable forced Rossby waves by EW, the top panels are zonal velocities, u, middle ones are meridional velocities, v, and the bottom ones are potential temperatures, θ.

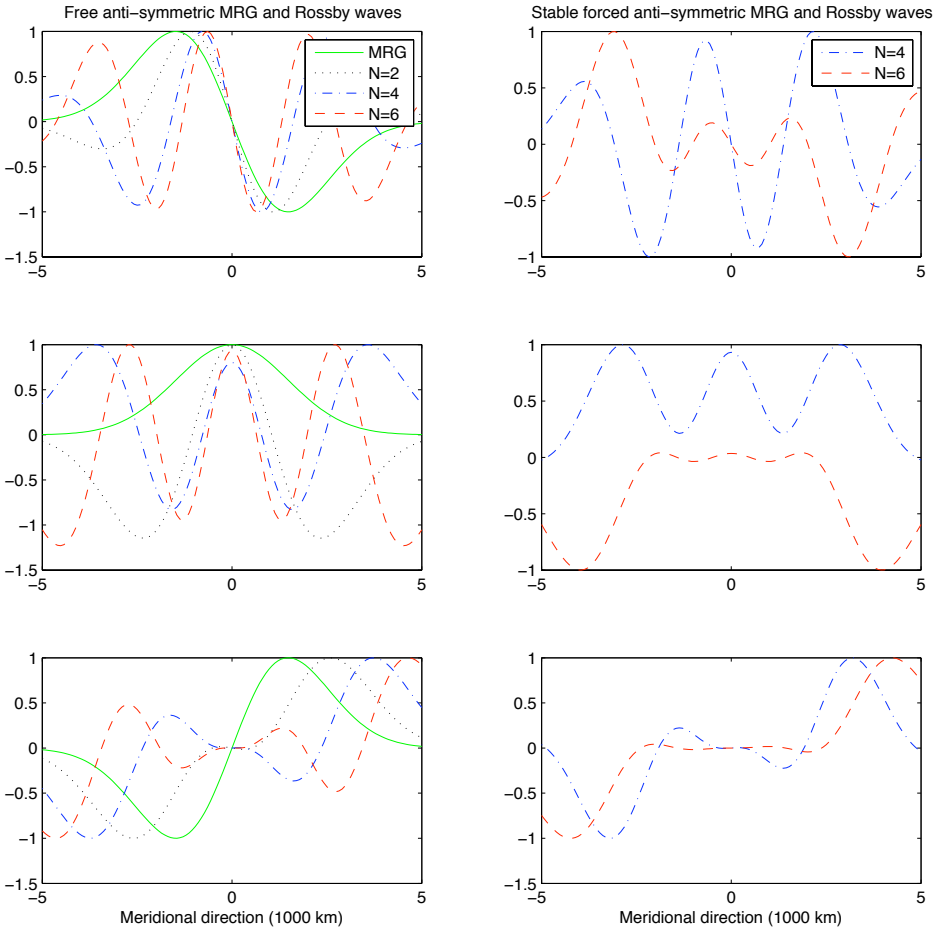

FIG. 12. Meridional structures of free anti-symmetric westward Yannai wave and Rossby waves with $N = 2, 4$ and 6. on the left side and the stable forced Rossby waves obtained westerly wind, the top panels are zonal velocities, u, middle ones are meridional velocities, v, and the bottom ones are potential temperatures, θ.

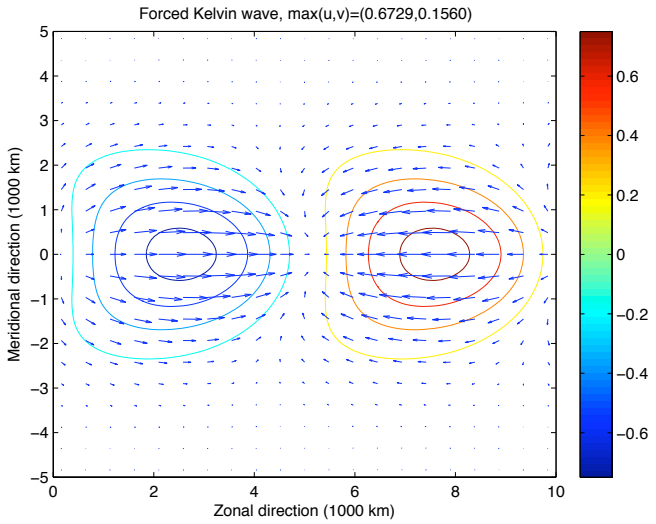

FIG. 13. Forced Kelvin wave with $k = 4$ in EE after 30 days, contours of the potential temperature and the flow (arrows)

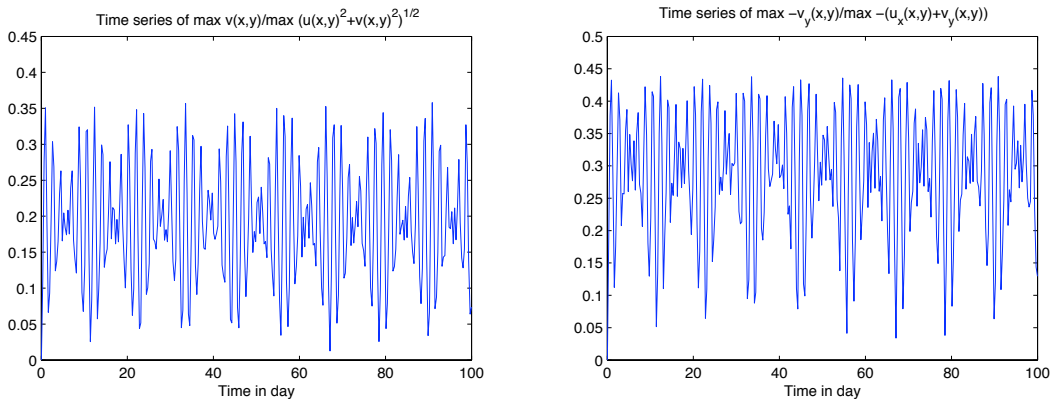

FIG. 14. Time series of the relative meridional wind (left) and relative meridional convergence (right)of the forced Kelvin wave $k = 4$.

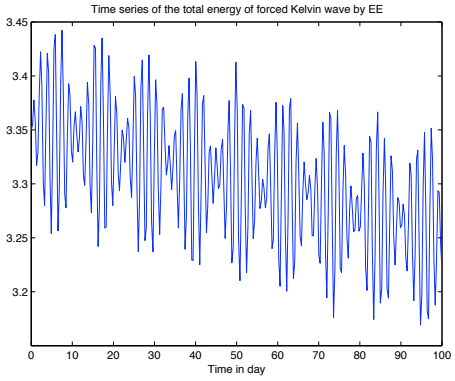

FIG. 15. Time series of the total energy of the forced Kelvin wave with $k = 4$ in EE.

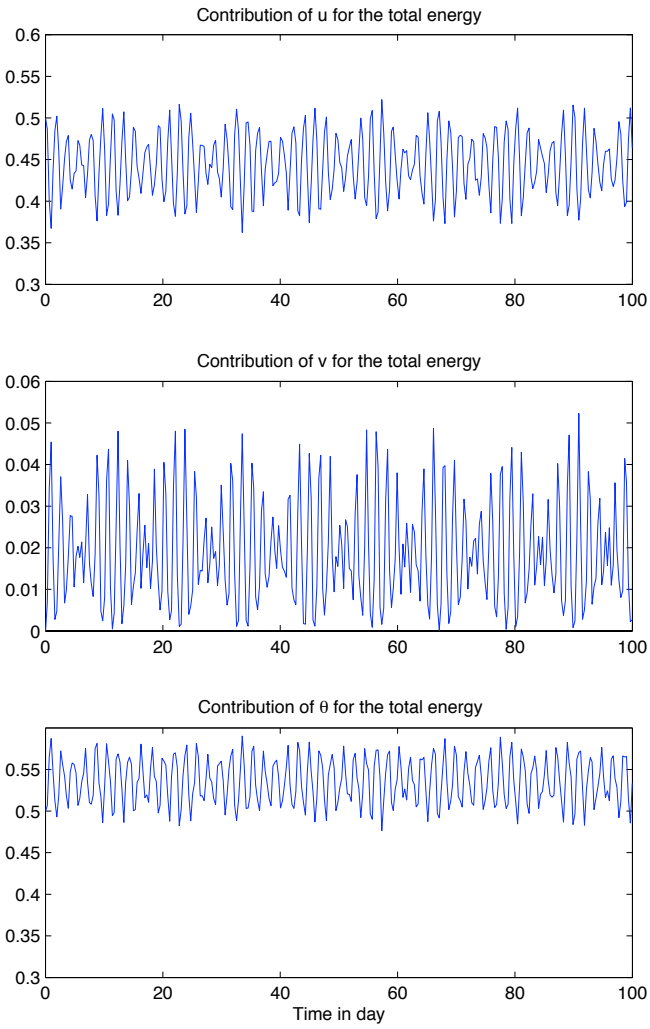

FIG. 16. Time series of contribution of u (top panel), v middle panel and θ bottom panel to the total energy of the forced Kelvin wave with $k = 4$ in EE.

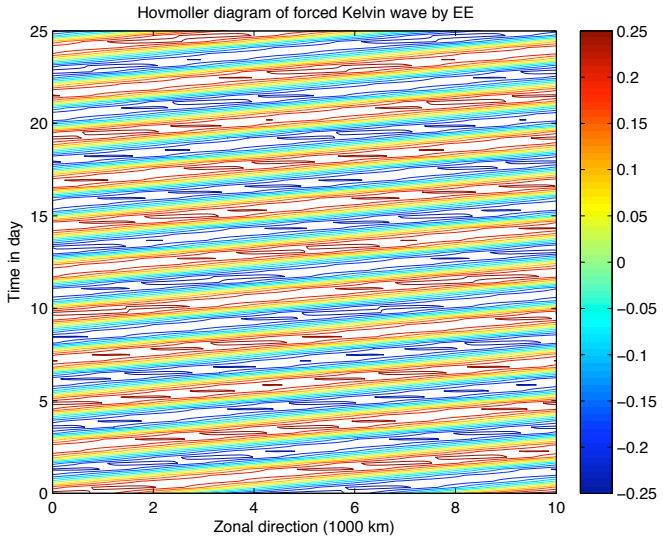

FIG. 17. Hovmoller diagram of the forced Kelvin wave with $k = 4$ in EE for [0-25] days.

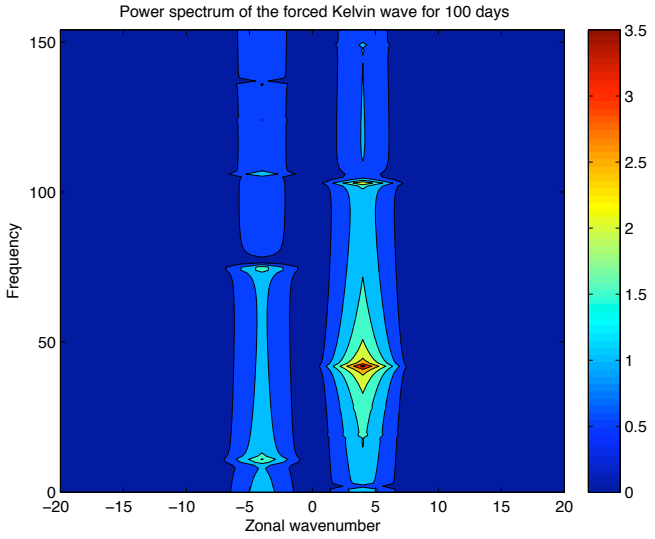

FIG. 18. Power spectrum in wavenumber-frequency obtained from the forced Kelvin wave $k = 4$ by EE.

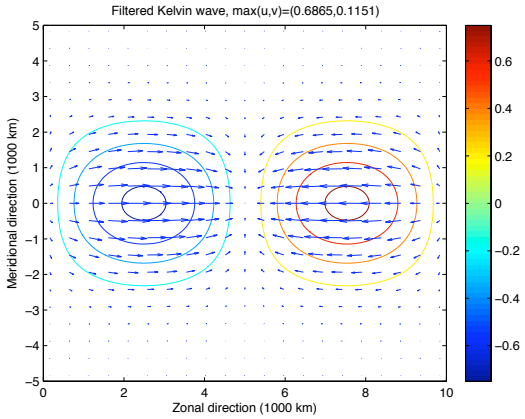

FIG. 19. Filtered Kelvin wave at t =30 days, contours of the potential temperature and the flow (arrows).

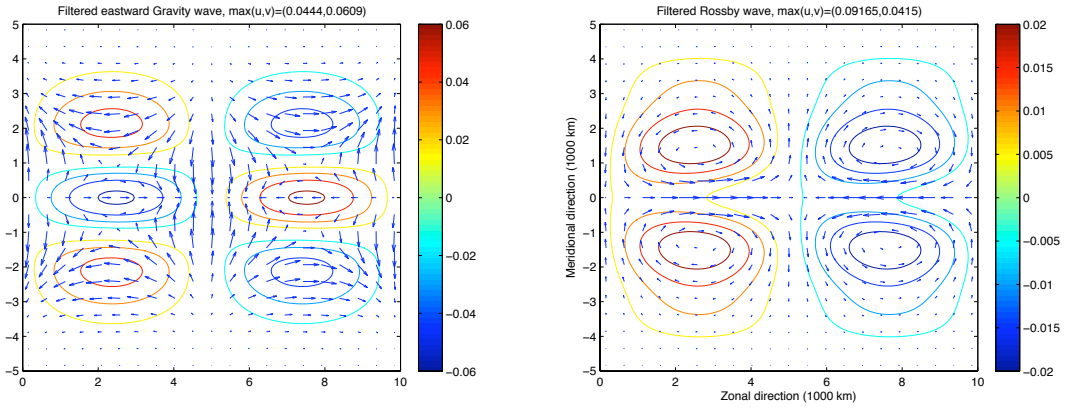

FIG. 20. Excited eastward Gravity (left panel) and excited Rossby wave at t =30 days, contours of the potential temperature and the flow (arrows).

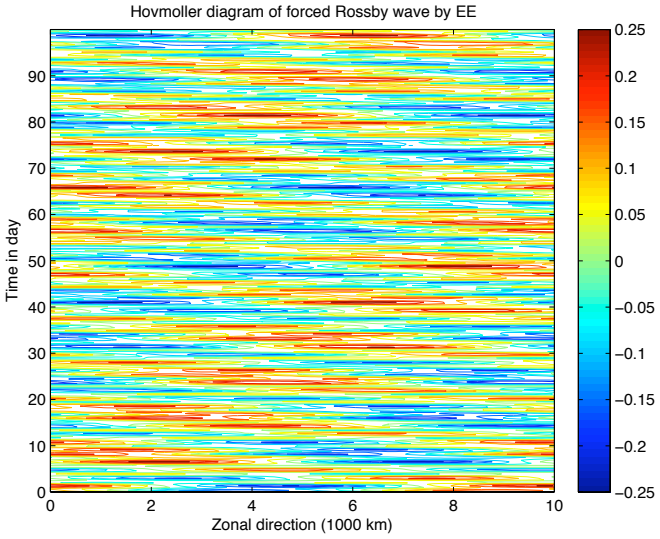

FIG. 21. Hovmoller diagram of the forced Rossby wave with $k = 4$ in EE.

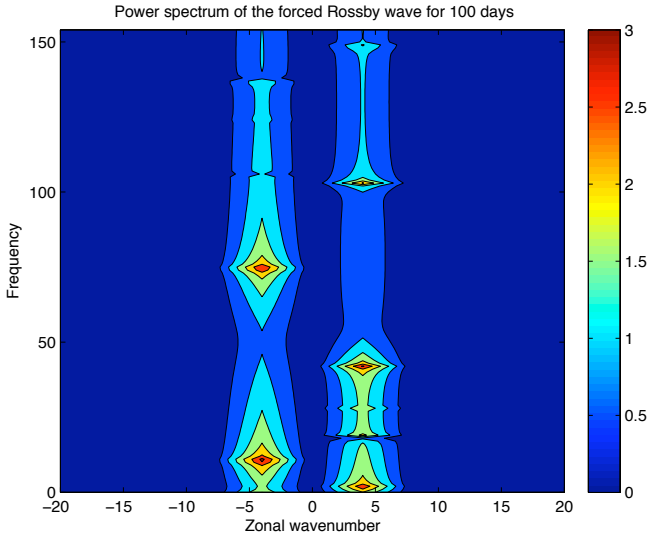

FIG. 22. Power spectrum in wavenumber-frequency obtained from the forced Rossby wave $k = 4$ by EE.

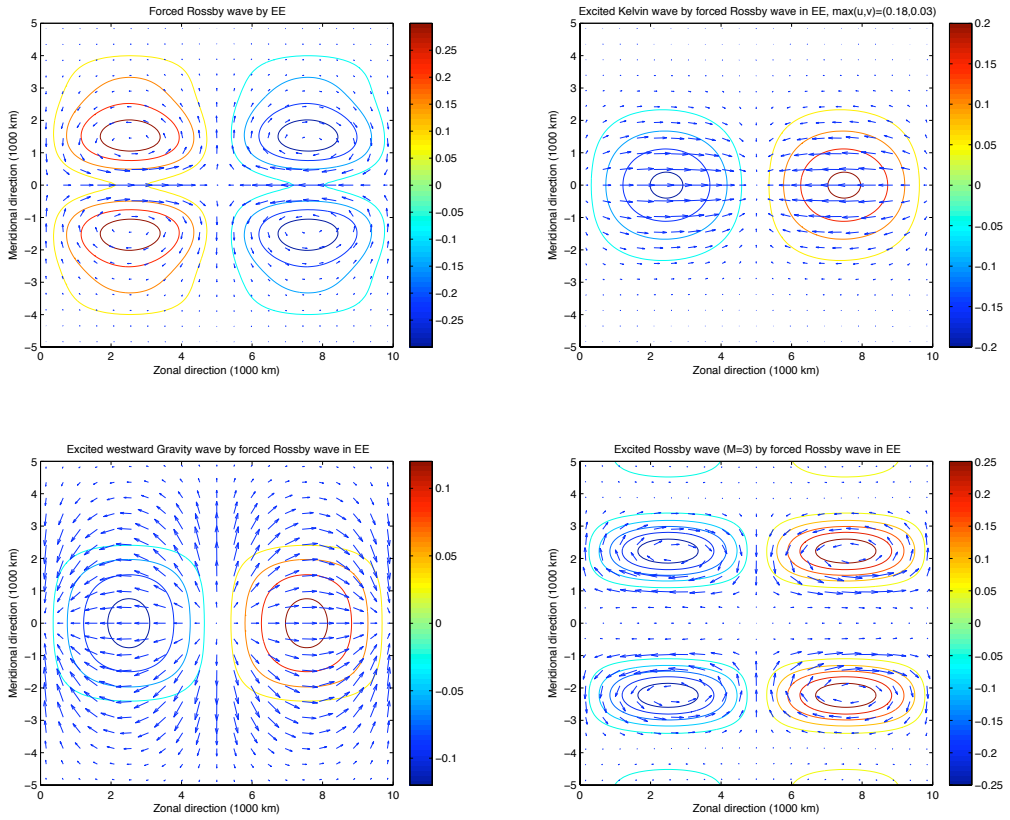

FIG. 23. Forced Rossby wave $M = 1$ (top-left), excited Kelvin wave (top-right) and excited westward Gravity wave (bottom-left) and excited Rossby wave $M = 3$ at t =30 days, contours of the potential temperature and the flow (arrows).

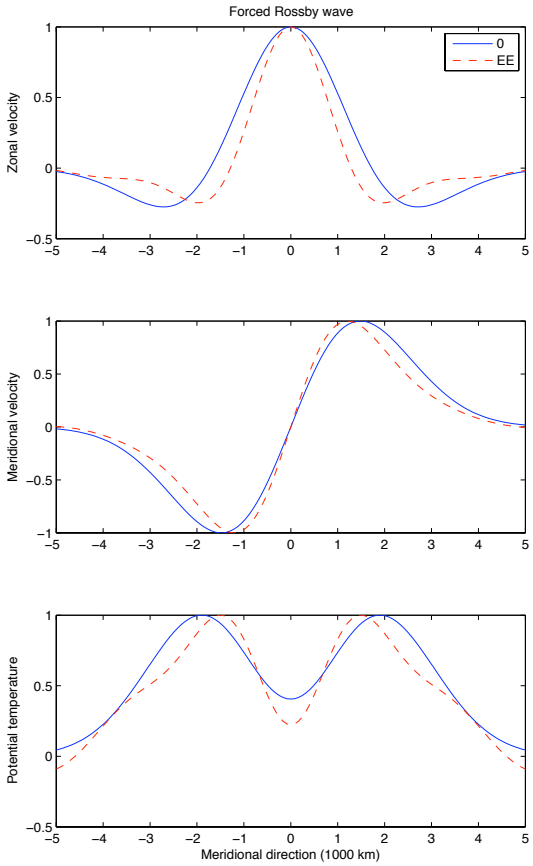

FIG. 24. Meridional structures of free symmetric Rossby waves with $M = 1$and forced Rossby waves by EE, zonal velocity (top panel), meridional velocities (middle panel) and potential temperatures (bottom panel).